



Full-scale load testing of two large-diameter drilled shafts in coral-reef limestone formations

Zhihui Wan^{1,2} · Guoliang Dai^{1,2} · Weiming Gong^{1,2}

Received: 20 June 2017 / Accepted: 9 November 2017 / Published online: 23 November 2017
© Springer-Verlag GmbH Germany, part of Springer Nature 2017

Abstract

Field load tests were conducted on two large-diameter drilled shafts in coral-reef limestone formations in the Male-Airport Island Cross-sea Bridge area in the Maldives. Due to the porosity of the rock mass, the degree of heterogeneity of the cementation, and the particle fragility of the coral-reef limestone in this area, the process of drilling a shaft weakens the side resistance and tip resistance of the shaft; thus, post-grouting was applied to strengthen the weakest zones of the natural coral. This paper presents the results of bi-direction O-cell testing on one 3.2 m diameter and one 1.5 m diameter drilled shaft before and after grouting in coral-reef limestone formations. Comparing with test results before and after grouting shows that the grouting enhanced both the shaft and tip resistance. The two test shafts had higher bearing capacity after grouting, and both of these values met the requirements of the shaft design. Additionally, post-grouting can be applied to coral-reef limestone formations and can effectively improve the bearing capacities of shafts and decrease their settlements. Finally, the research results were directly applied to the design of a bridge foundation and may be applicable to similar projects in coral-reef limestone formations.

Keywords Coral-reef limestone · Drilled shaft · Osterberg cell method · Post grouting · Shaft resistance · Tip resistance

Introduction

Drilled shafts have been widely used in high-rise buildings and highway bridges because of their high bearing capacity, easily adjusted depth and low environmental pollution. However, soil relaxation beneath the shaft tip due to the drilling process, heavily influences the tip resistance, which is reduced even further by debris remaining after cleanout (Sliwinski and Fleming 1984; Mullins et al. 2000; Dapp and Mullins 2002; Safaqah et al. 2007). Additionally, release of soil stress and disturbances surrounding the shaft due to drilling will also reduce the side friction (O’Neill and Reese 1976; Majano et al. 1994; Sliwinski and Philpot 1980; Dapp et al. 2006; Safaqah et al. 2007; Zhang et al. 2009). Hence, the construction process has a negative impact on the bearing capacity of drilled shafts. Furthermore, the tip resistance and shaft resistance cannot develop simultaneously. The shaft

resistance is fully mobilized at displacements between 0.5 and 1.0% of the shaft diameter (D), but tip resistance fully develops at displacements of 10–15% D (Bruce 1986; Hirayama 1990; Mullins et al. 2000). Therefore, the displacement required to the mobilized tip resistance is much larger than that of shaft resistance. The tip resistance is not fully mobilized within the service displacement limits even in ideal conditions.

Coral-reef limestone is formed by marine plants (corals) and marine animals (coral algae) over long geological processes (Deshmukh et al. 1985). These formations generally have a heterogeneous nature, structural variability, low bulk density and cementitious properties, resulting in their possessing distinctive geotechnical characteristics that are significantly different from those of other terrigenous soils (Agarwal et al. 1977; Ghazali et al. 1987; Poulos 1989). The process of shaft drilling disturbs the rock immediately surrounding the shaft and causes subsequent movement of some crushed particles into the adjacent porous formation. Consequently, very low lateral pressures are developed against the surface of the shaft, producing very low side friction and tip resistance of the shaft (Ghazali et al. 1988). Pressure grouting is considered necessary to increase adhesion of concrete to the coral-reef limestone formation. Additionally, the pores and holes in rock are filled with

✉ Guoliang Dai
daigl@seu.edu.cn

¹ Key of Laboratory for RC and PRC Structure of Education Ministry, Southeast University, Nanjing 210096, China

² School of Civil Engineering, Southeast University, Nanjing 210096, China

pressurized grout to improve the weakest zones of the natural coral, yielding high side friction and tip resistance of the shaft (Nauroy and LeTirant 1985; Gunasena et al. 1995; Joer et al. 1998). Hence, the construction defects of the drilled shaft are eliminated, and the engineering properties of the weak geology are improved by post-grouting. Post-grouting techniques have been used widely throughout the world and have proven to be an effective method to improve axial resistance and reduce settlement (Bolognesi and Moretto 1973; Bruce 1986; Mullins et al. 2001; Mullins et al. 2006; Dapp et al. 2006; Safaqah et al. 2007; Dai et al. 2010; Thiyyakkandi et al. 2014).

At present, the static load test is the most direct and effective approach to study the bearing behavior of a shaft. It has been reported by many authors (Dai et al. 2010; Zhang and Zhang 2012; Nguyen and Fellenius 2015; Liu et al. 2015) that the influence of post-grouting on the bearing behavior of a compressive shaft has been analyzed on the basis of static test results of a shaft field test. However, there are few investigations of the bearing behaviors of shafts in coral-reef limestone formations, especially full-scale load tests after post-grouting craftwork has been applied. Owing to their special complexity, it is necessary to carry out the bi-directional O-cell tests of the grouted shafts in coral-reef limestone formations. Bi-directional O-cell tests were introduced by Osterberg (1986) and employed in the first practical engineering in 1987; it was subsequently developed and applied extensively throughout the world (Choi et al. 2016).

This paper reports full-scale load tests to investigate the field performance of two large-diameter drilled shafts before and after grouting in coral-reef limestone formations in the context of a practical bridge engineering problem. Bi-directional O-cell tests were conducted to determine the bearing capacity of the shafts before and after grouting. The axial force distribution, shaft resistance, the relationship between the shaft resistance and relative displacement and tip resistance, and the effect of post-grouting under axial compression load in the coral-reef limestone formations are estimated from the strain gauge data and are compared with measurements obtained for the ungrouted shaft.

Project description

The Male-Airport Island Cross-sea Bridge is the most important connection project in the Maldives. The bridge, which connects Male City and Airport Island, will be the first cross-sea bridge in the Maldives. It will have a width of 21 m and a total length of 2000 m, of which the lengths of the main and approach bridges will be 760 m and 630 m, respectively. The proposed bridge, which needs to bear a heavy load, will be large. It will be difficult to achieve the load requirement by adopting a natural or extended pier

foundation. Consequently, following various comprehensive analyses of the engineering characteristics, site conditions and construction factors, drilled shafts are to be used as the foundations of the bridge. The foundations for piers No. 19–21 and No. 22–23 of the main bridge are each composed of 12 nos. of 3.2 m diameter and 8 nos. of 2.8 m diameter drilled shafts, respectively, while the foundation for the piers of the approach bridge are each composed of 6 nos. of 1.5 m diameter drilled shafts. The deepest seabed is 46.17 m from the sea surface. The layout of the main bridge is illustrated in Fig. 1.

Site and test shaft conditions

The geology of the site area was examined prior to the design of the pile foundations. From geological drilling,

the distribution of the superficial zone is filled with coral gravel and residual limb in the test site exploration depth of 100 m. The geological layer of the site area consists of Holocene loose coral with sand Pleistocene reef rock and weakly cemented or unconsolidated coral with sand. The location of the site investigation near the test shafts is shown in Fig. 2. In Fig. 2, borehole BH2 is located 19.43 m and 22.35 m from the test shafts TS2 and TS3, respectively. The soil profile (Figure 3) consists of the following seven types of rocks and soils: (1) a 2.7-m-thick fill at the surface, (2) gravel with coral fragments approximately 4.7-m-thick between 2.7 and 7.4 m from the ground surface, (3) 4.6-m-thick reef rock with coral fragments or coral gravels between 7.4 and 12 m, (4) a total of 28.9 m of massive reef rock in five layers, located at depths of 12–20 m, 20–25.2 m, 36–40 m, 45.7–53.4 m, and 80–84 m, (5) 10.8-m-thick reef rock with cavities between 25.2 and 36 m, (6) a total of 22.3-m-thick massive reef rock with cavities in two layers, located at depths of 40–45.7 m and 53.4–70 m, and (7) a total of 26-m-thick crushed reef rock with gravel in two layers, located at depths of 70–80 m and 84–100 m. Details of the rock and soil layers at the site and the corresponding average physical properties are listed in Table 1, in which ρ_{sat} is the saturated density of each rock and soil layer, V_s and V_a are the shear wave velocity and acoustic wave velocity, respectively, of each rock and soil layer derived from in situ tests, SPT N and DPT N are the blowcounts of the standard penetration tests and dynamic penetration tests, respectively, and I_s and R_c are the point load strength and uniaxial compressive strength obtained from point load tests and uniaxial compression tests, respectively. Because of the peculiar and unusual behavior of the coral-reef limestone formations, the physical properties of some rock and soil layers were not obtained; the average physical properties of rock layers with the same name but located in different areas may be different from each other due to the heterogeneity of coral-reef limestone formations.

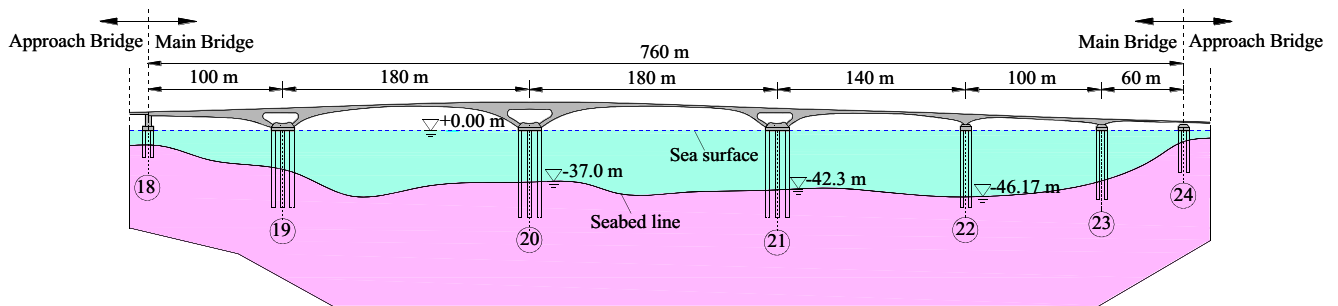


Fig. 1 Layout of main bridge

Coral-reef limestone is the main stratum of a coral-reef island and is the bearing stratum of the proposed bridge foundation. Reef rocks are formed by remains of coral and coral-line algae through filling, cementation, biological encroachment, sedimentation and other marine dynamics processes. The processes finally form a type of geotechnical material with a certain compact degree and structural strength. Research results show (Wang et al. 1997) that coral-reef limestone is a complex and special material with strong biological characteristics, and it has extreme heterogeneity and structural uniqueness. Additionally, coral-reef limestone has regional characteristics, and the structural properties and cementation degree of coral-reef rocks are different even within the same coral-reef island due to sedimentary facies evolution and the historical sedimentary environment. From the core analysis of the site, the particularity of the coral-reef limestone in the field area mainly includes the porosity of the rock mass, the complexity of the particle space, the heterogeneity of the degree of cementation and the particle fragility. Site core samples are shown in Fig. 4.

Owing to the special complexity of coral-reef limestone formations, there is little experience with this type of rock formation in bridge foundation engineering. To provide a

useful reference for the design and to guide the construction of the main approach bridge, it was necessary to carry out the shaft tests in the proposed project area. The test shafts TS2 and TS3 were 3.2 m and 1.5 m in diameter and 44 m and 19 m deep, respectively, and were both constructed by rotary drilling. Shafts TS2 rested on a layer of crushed reef rock with gravel and TS3 rested on a layer of reef rock with cavities. The elastic modulus of the concrete for the two test shafts E_c was 31.5 GPa. From the requirements of the estimated bearing capacity and the soil layer within the shaft length of the main approach bridge, concrete was not poured from the surface to 46 m and 10.4 m below the natural ground level for shafts TS2 and TS3, respectively. To accommodate the requirements of the sensor arrangement, 52 and 35 reinforcing bars with respective diameters of 32 mm and 25 mm were attached along the lengths of the test shafts TS2 and TS3. The post-grouting technique of the shaft tip-and-side combination and a single shaft tip were applied to the test shafts. Four straight grouting pipes at the shaft bottom and two ring-shaped grouting pipes at the shaft side were adopted for test shaft TS2, and three straight grouting pipes at the shaft bottom were adopted for test shaft TS3. The grouting system is the same as that described by Duan and Kulhawy (2009). The grouting pipe

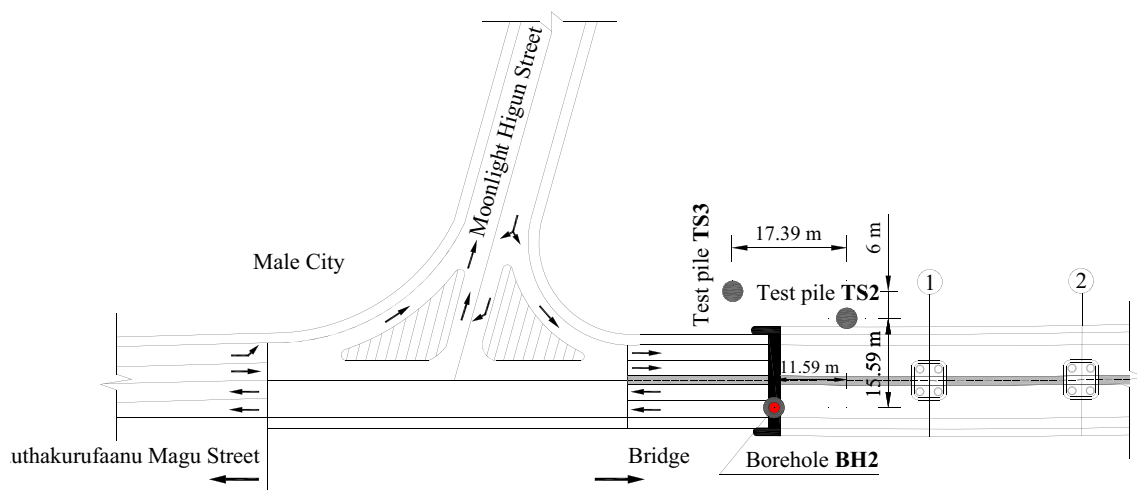
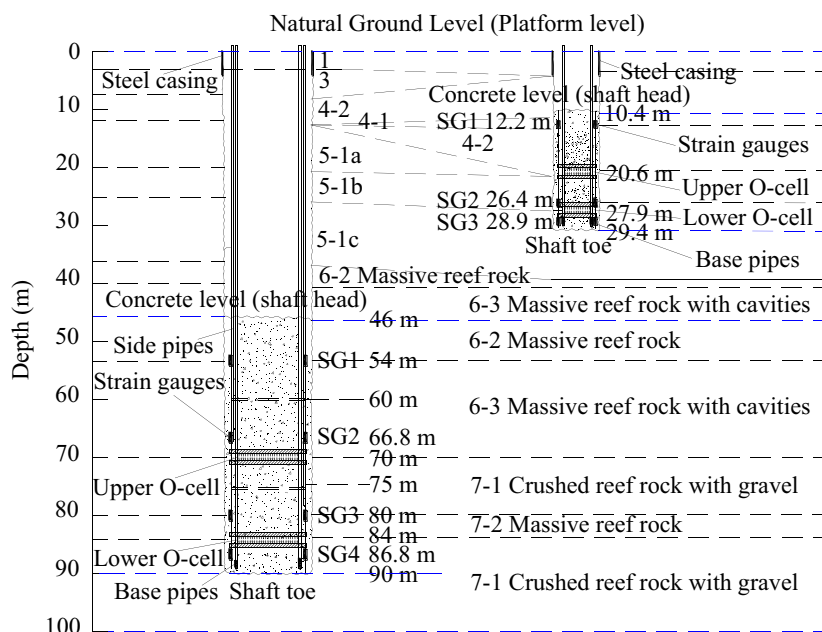


Fig. 2 The location of test piles and borehole BH2

Fig. 3 Distribution of soils and locations of strain gauges



Note: The names of the detailed rock and soil layers are shown in Table 1.

layout of test shafts is shown in Fig. 3. The figure shows that the first and second ring-shaped grouting pipes at the shaft side were located at depths of 60 and 75 m, respectively (i.e., 30 and 15 m above the shafts' tips). To investigate the mechanism of load transfer of the grouted shafts in coral-reef limestone formations, the shafts were instrumented with vibrating wire strain gauges at various locations along the shafts' lengths. The strain gauges were installed on the four symmetrical reinforcing bars at each instrument level. The instrumentation details of the test shafts are presented in Fig. 3.

Field test

The bi-direction O-cell test

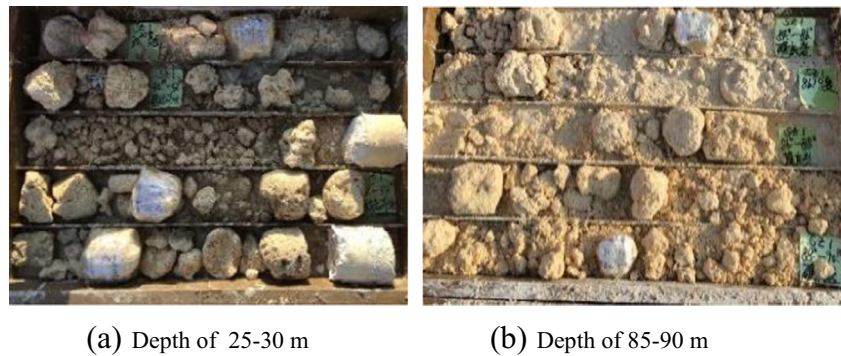
Top-down load test methods require thousands of tons of material or a heavy reaction frame. However, the deficiencies of top-down load tests can be overcome by the bi-direction O-cell test, which was thus adopted for this case. It is difficult to meet the requirement of the bearing capacity of the design shaft with the single-level O-cell bi-direction test because of the particularity of the coral-reef limestone formations.

Table 1 Physical properties of the different rock and soil layers

Soil no.	Rock and soil layer	ρ_{sat} (g/cm ³)	V_s (m/s)	V_a (m/s)	SPT N	DPT N	I_s (MPa)	R_c (MPa)
1	Fill	–	207	1014	–	7	–	–
3	Gravel with coral fragments	–	228	1355	21	12	–	–
4-1	Reef rock with coral gravel	2.21	398	1990	76	69	3.45	10.73
4-2	Reef rock with coral fragments	–	364	1747	25	26	2.87	–
5-1a	Massive reef rock	2.40	606	2219	–	–	2.33	10.20
5-1b	Massive reef rock	2.22	626	2876	–	–	2.47	7.50
5-1c	Reef rock with cavities	2.29	432	2146	–	–	1.91	5.93
6-2	Massive reef rock	2.25	628	2530	–	31	2.83	8.42
6-3	Massive reef rock with cavities	2.23	587	2587	–	32	2.73	5.53
7-1	Crushed reef rock with gravel	2.20	589.5	2959	53	–	2.40	5.18
7-2	Massive reef rock	2.12	610	2790	–	–	2.59	10.35

Note: The names of the detailed rock and soil layers are shown in Table 1

Fig. 4 Core samples at site



Therefore, double-level O-cell of the bi-direction test method was employed for this test. The shaft was divided into upper, middle and lower segment by a double-level O-cell. Figure 5 presents a schematic showing the double-level O-cell details. The detailed loading procedure was as follows. First, the upper O-cell was locked and the lower O-cell was loaded to measure the relationship between the load and displacement of the lower shaft segment (Stage 1). Second, the lower O-cell was opened and the upper O-cell was loaded to measure the relationship between the load and displacement of the middle shaft segment (Stage 2). Finally, the lower O-cell was locked, and then the upper O-cell was continuously loaded to failure (Stage 3). The order of the upper O-cell and lower O-cell tests in the bi-directional double-level O-cell tests method was determined by the position of the double-level O-cell, the soil conditions and the test requirements. The upper level was 20 m above the shaft tip in test shaft TS2 with a total nominal ultimate load of 100 MN, while the lower level was 6 m above the shaft tip with a total nominal ultimate load of 100 MN. The upper level was 8.8 m above the shaft tip for test shaft TS3 with a total nominal ultimate load of 30 MN, while the lower level was 1.5 m above the shaft tip with a total nominal ultimate load of 30 MN. The positions of the double-level O-cells for both shafts are illustrated in Fig. 3. The bi-directional double-level O-cell tests for both shafts were conducted before and after grouting.

The bi-directional double-level O-cell tests were conducted on the test shafts in accordance with a slowly maintained load procedure. The methods of loading and unloading followed the Chinese standard JT/T 738–2009 (The Traffic Professional Standards Compilation Group of People's Republic of China 2009). The loading termination criteria were as follows: (1) The displacement was equal to 40 mm or more; in this loading grade, with a displacement of five times the previous displacement or more, the test can terminate loading. The previous loading is deemed to be the ultimate bearing capacity. (2) The total displacement is 40 mm or more; in this loading grade, if stabilization is not achieved within 24 h, the test can terminate loading. The previous loading is deemed to be the ultimate bearing capacity. (3) If the

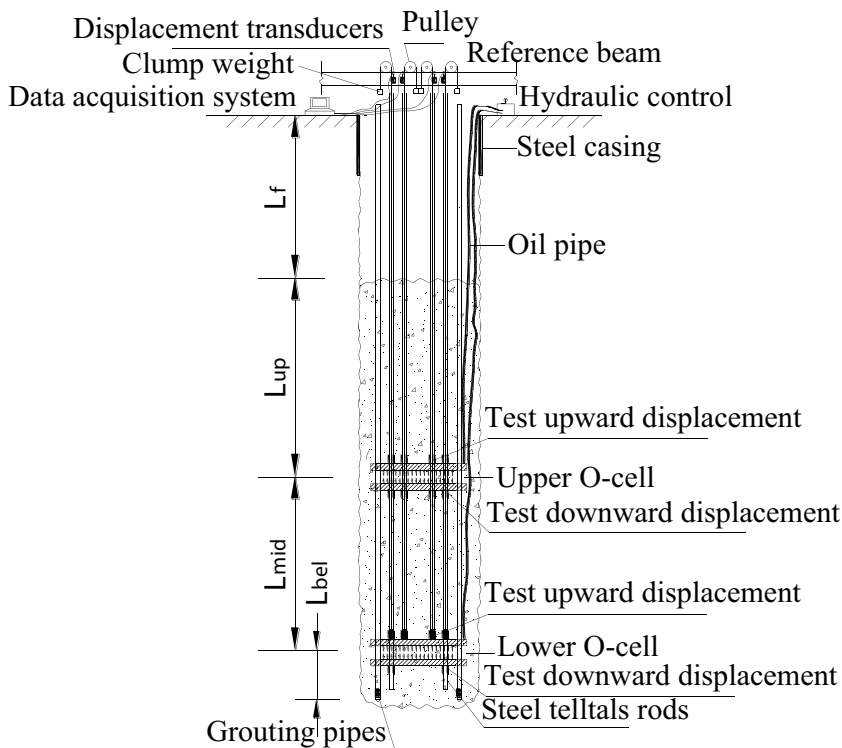
total displacement is less than 40 mm, but the loading reaches the ultimate capacity of the load cell and/or it exceeds the range of the load cell, loading can be terminated. Two displacement transducers were fixed at the top of the shaft and four displacement transducers were installed at the upper and lower levels of the O-cell, as shown in Fig. 5a. A photograph taken during the installation of the Osterberg load cell and vibrating wire gauges is shown in Fig. 5b. Figure 5c is a photograph taken after the lower O-cell was attached to the steel rebar cage of the designated shaft when the device was being lowered in the pre-drilled shaft.

The test process

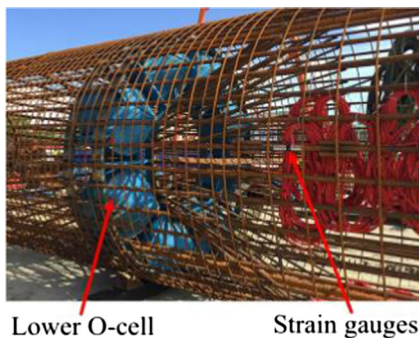
The test shaft TS2

The bi-directional double-level O-cell test was conducted in two phases: before and after grouting. The first phase commenced on September 3, 2016 and was conducted 7 days after pouring the concrete. First, the lower O-cell was closed and the upper O-cell was loaded to measure the relationship between the load and displacement of the upper shaft segment before grouting. In the first stage, the upper O-cell was loaded in 20 loading increments, each of 5 MN and 120 min duration. At the end of the 20th increment, the upper O-cell load was approximately 100 MN; the downward and upward displacements were 11.16 mm and 15.45 mm, respectively. When the upper O-cell reached the load limit (total nominal ultimate load of 100 MN), the loading was terminated. At the end of the first stage test, the test shaft was unloaded in five increments. The resting period for the loading of the lower O-cell was not less than 24 h after the first stage test. The lower O-cell was loaded to measure the relationship between the load and displacement of the middle and lower shaft segments before grouting. In the second stage, the upper O-cell was opened, and the lower O-cell was pressurized in 19 loading increments. Upward displacement cannot reach stabilization; thus, in the third stage, the upper O-cell was closed and the lower O-cell was loaded in 20 loading increments. When the lower O-cell load was approximately 100 MN with downward displacement of 52.34 mm, the loading was terminated. At the

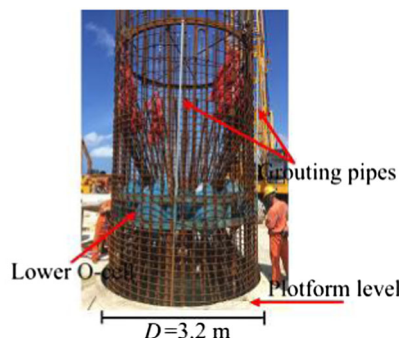
Fig. 5 Sketch and on-site photographs of double-level load cell for bi-directional test for shaft



(a) The sketch of double-level load cell



(b) Installation of Osterberg load cell



(c) Lowering steel cage

end of the third stage test, the test shaft was unloaded in five increments.

The grouting stage was conducted immediately after the first phase test was completed. The test shaft TS2 was subjected to combined grouting at the shaft tip and side. Soil conditions are key to determining the grout material, followed by environmental conditions, the purpose of grouting and other factors. Ordinary Portland cement should not be adopted in coral-reef limestone formations due to its porosity and connected holes. The Maldives is a natural reserve, where sodium silicate and other polluting grouting materials cannot be used. Therefore, a special grouting material composed of cement, a special admixture, polymer material and a variety of mineral

modified materials, was used. The amount of grout and the grouting pressure were both controlled during the grouting process; the grouting parameters of test shaft TS2 are given in Table 2.

The second phase was conducted 20 days after the combined grouting. The procedure was the same as the first phase. In the first stage, the upper O-cell load was approximately 100 MN; downward and upward displacements were 5.63 mm and 9.06 mm, respectively. The upper O-cell reached the load limit, and then the loading was terminated. At the end of the first stage test, the test shaft was unloaded in five increments. In the second stage, the upper O-cell was opened, and the lower O-cell was loaded in 20 increments. The lower O-cell

Table 2 Grouting parameters of test shaft TS2

Shaft no.	Water/cement ratio	Quantity of cement (kg)			Grouting pressure (MPa)		
		First	Second	Shaft tip	First	Second	Shaft tip
TS2	0.27	400	2040	3720	4.6	6.7	7.2

Note: First and Second denote the first and second ring-shaped grouting pipes at the side of the shaft, respectively

load of 100 MN was achieved with downward displacement of 46.79 mm, and the loading was terminated. The test shaft was unloaded in five increments, and the test was stopped.

The test shaft TS3

The first phase commenced on September 28, 2016 and was conducted 7 days after pouring the concrete. First, the upper O-cell was closed and the lower O-cell was loaded to measure the relationship between the load and displacement of the lower shaft segment before grouting. In the first stage, the lower O-cell was loaded in six loading increments; each increment was 1.5 MN and lasting 120 min. At the end of the sixth increment, the lower O-cell load was approximately 9 MN with downward displacement of 72.47 mm, and the loading was terminated. Thus, the ultimate bearing capacity of the lower shaft segment was 7.5 MN. At the end of the first stage test, the test shaft TS3 was unloaded in five increments. The resting period for loading the upper O-cell was not less than 24 h after the first stage test. The upper O-cell was loaded to measure the relationship between the load and displacement of the lower shaft segment before grouting. In the second stage, the upper O-cell was pressurized in 20 loading increments. At the end of the 20th increment, the upper O-cell load was approximately 30 MN, with downward and upward displacements of 8.23 mm and 7.12 mm, respectively. The upper O-cell reached the load limit (total nominal ultimate load of 30 MN), and the loading was terminated. At the end of the second stage test, the test shaft was unloaded in five increments.

The grouting stage was conducted immediately after the first phase test was completed, and the test shaft TS3 was grouted at the shaft tip. The grout used was 3170 kg, and the grouting pressure was approximately 2.2 MPa.

The second phase was conducted identically to the first phase 20 days after the tip grouting. In the first stage, after the eighth loading increment, the lower O-cell load of 12 MN was achieved with downward displacement of 49.83 mm. In the second stage, at the end of the 20th increment, the upper O-cell load was approximately 30 MN with downward and upward displacements of 8.59 mm and 7.05 mm, respectively. When the upper O-cell reached the load limit, the loading was terminated. The test shaft was unloaded in five increments, and the test was stopped.

Analysis of loading-test results

Load versus displacement

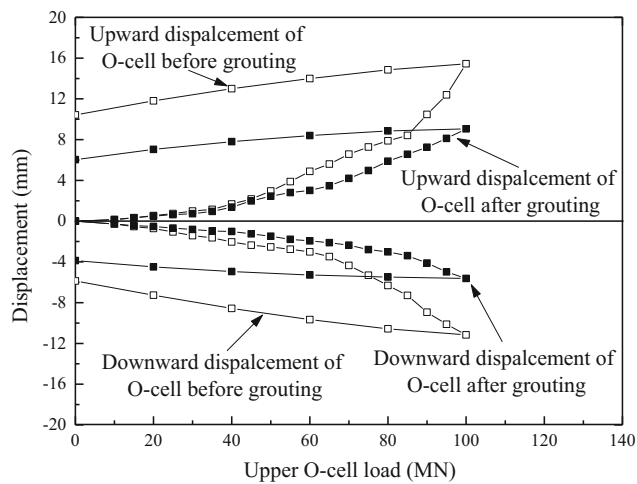
The measured load-displacement curves of TS2 and TS3 before and after grouting are shown in Figs. 6 and 7. The downward and upward displacements of the O-cell and the proportion of the total displacement by the rebound displacement after unloading of TS2 and TS3 before and after grouting is shown in Table 3.

It can be observed from Figs. 6 and 7 that there is almost no displacement of each shaft segment at light loading levels. The displacement of each shaft segment increases gradually with increasing load. At the maximum loading level, the load-displacement curves of the lower shaft segment have a clear inflection point, but the shaft resistances of the upper and middle shaft segments have not been fully mobilized. The graphs show that the actual ultimate bearing capacities of the upper and middle shaft segments are larger than the test load. They also reflect that the reef limestone formations in this area have a high bearing capacity, and the requirements of the shaft design can be achieved.

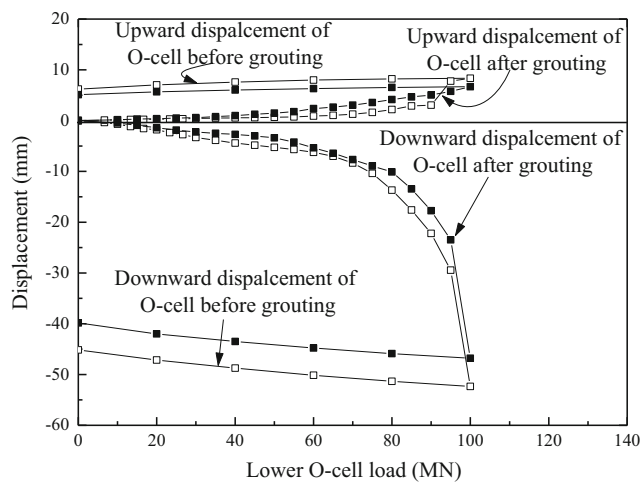
It can also be found from Fig. 6 that the displacement of a grouted shaft is lower than that of an ungrouted shaft, which demonstrates that the post-grouting technique of the shaft tip-and-side combination can effectively control settlement of the shaft in these coral-reef limestone formations. It can be observed from Fig. 7 (b) that the trends of lower O-cell load-displacement curves before shaft grouting are similar to those after grouting. Under the ultimate load, the ultimate bearing capacity of the lower shaft segment after grouting was increased by 40%, which indicates that the tip grouting technique can significantly improve the bearing capacity of the shaft in the coral-reef limestone formations. The bearing capacity of the grouted shaft is larger than that of the ungrouted shaft at the same displacement, and can be mobilized at a much smaller displacement. Consequently, the bearing behavior of the shaft is effectively improved by post-grouting craftwork, producing high capacity and low shaft settlement in the coral-reef limestone formations.

Equivalent conversion results

The results of the double-level bi-direction O-cell test before and after grouting were converted into the equivalent shaft

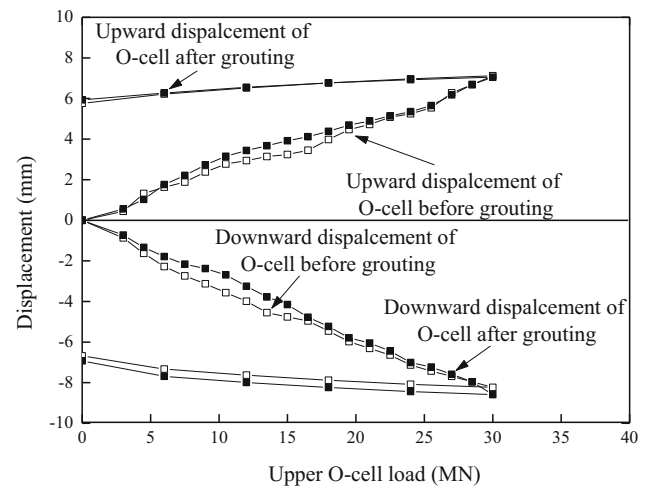


(a) Upper O-cell

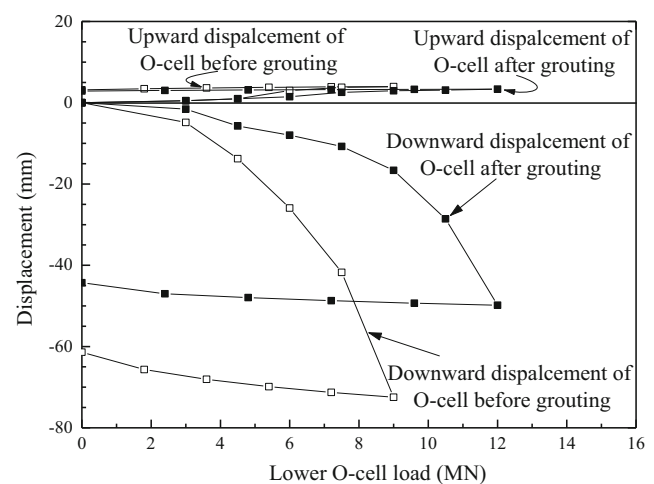


(b) Lower O-cell

Fig. 6 Test curves for test shaft TS2 before and after grouting



(a) Upper O-cell



(b) Lower O-cell

Fig. 7 Test curves for test shaft TS3 before and after grouting

head load-displacement curves for the top-down load-test method. The details of the equivalent conversion of the bi-direction O-cell test method were discussed by Dai et al. (2010). Thus, the equivalent shaft head load-displacement curves of the test shafts before and after grouting are obtained, as shown in Fig. 8.

Figure 8 shows that the equivalent load-displacement curves of the test shaft TS2 before and after grouting have distinct plunging points, whereas no sharp drops occur between the curves of the test shaft TS3 before and after grouting. That is, the load applied to the test shaft TS3 is considerably less than its ultimate bearing capacity. Prakash and Sharma (1990) and Zhang et al. (2014) have proposed that the ultimate bearing capacity of a single shaft is taken to be the load when the shaft plunges. Thus, the load prior to reaching the maximum load can be regarded as the ultimate bearing capacity, i.e., when the equivalent applied load at the test shaft

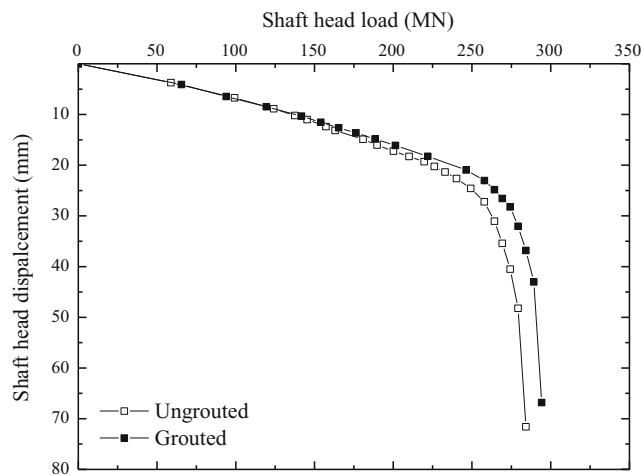
TS2 head before post-grouting is loaded from 279.29 MN to 284.29 MN, the equivalent displacement at the shaft head sharply increases. Therefore, the ultimate loads of the test shafts TS2 and TS3 before and after grouting are 279.29 MN, 294.29 MN, 67.24 MN, and 70.24 MN, respectively. The test results indicate that the bearing capacities of both shafts fully meet the requirements of the design load. Compared with the test results before grouting, the ultimate bearing capacity of the test shafts after grouting in coral-reef limestone formations increases. In addition, the equivalent displacements at shaft head of the test shaft TS2 at load levels of 279.29 MN before and after grouting were 48.22 mm and 32.05 mm, respectively, whereas the equivalent displacements at shaft head of the test shaft TS3 at load levels of 67.24 MN before and after grouting are 26.88 mm and 22.22 mm, respectively. Note that the shaft head displacements of the test shafts TS2 and TS3 were reduced by 16.17 mm and 4.66 mm

Table 3 The loads and settlements of test shafts

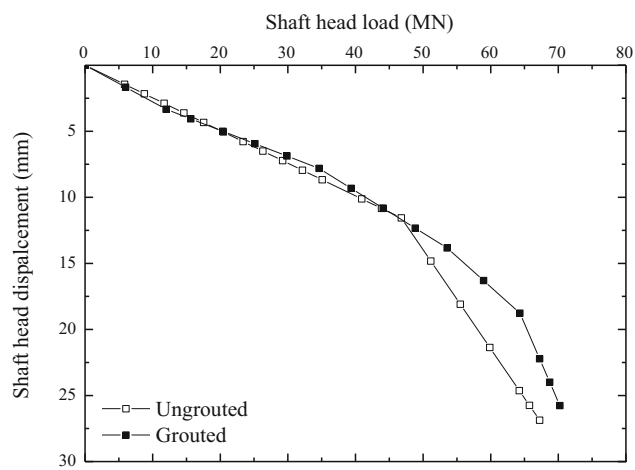
Shaft no.	Grouting situation	Load (MN)	Total displacement (mm)		Proportion of the total displacement by the rebound displacement (%)	
			Upward	Downward	Upward	Downward
TS2	UngROUTed	Upper O-cell 100	15.45	11.16	32.49	47.40
		Lower O-cell 100	8.33	52.34	25.33	13.72
	Grouted	Upper O-cell 100	9.06	5.63	33.33	31.26
		Lower O-cell 100	6.69	46.79	23.47	14.85
TS3	UngROUTed	Upper O-cell 30	7.12	8.23	19.10	18.83
		Lower O-cell 9	3.97	72.47	20.40	15.30
	Grouted	Upper O-cell 30	7.05	8.59	15.87	19.32
		Lower O-cell 12	3.34	49.83	13.77	11.08

due to post-grouting, which are 33.53% and 17.34% of the total displacement at the shaft head before grouting. The

results show that the combined grouting at the shaft tip and side to reduce the shaft head settlement is more effective than the grouting at the shaft tip alone.



(a) TS2



(b) TS3

Fig. 8 Equivalent load versus settlement curves of test shafts before and after grouting

Load distributions

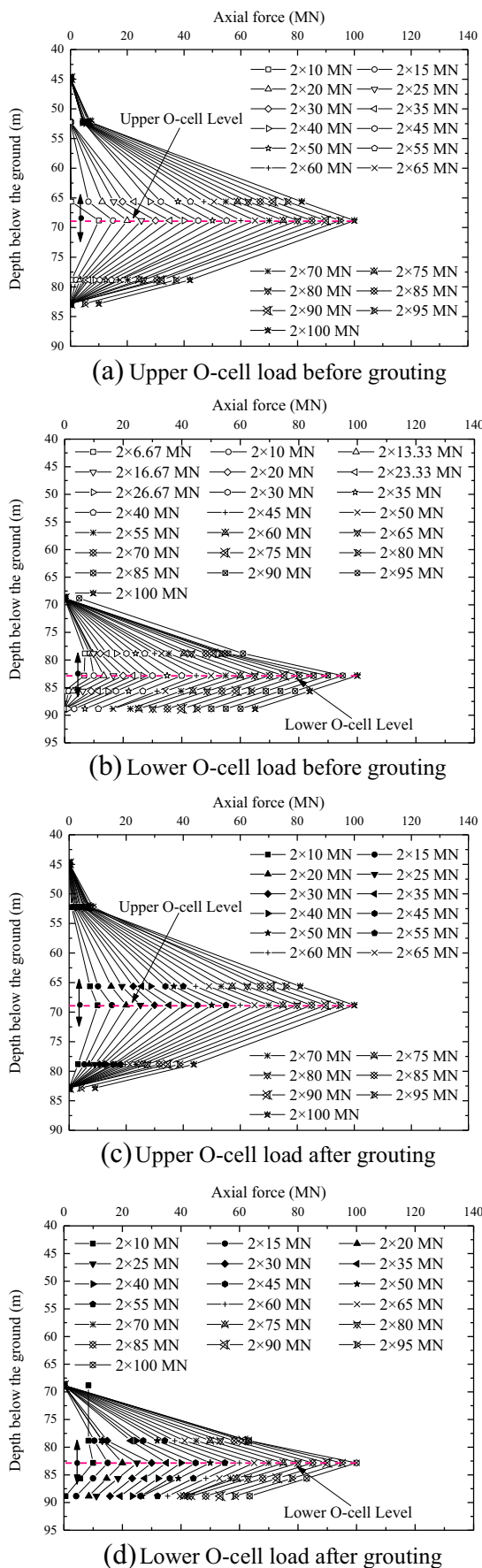
From the measured vibration frequency of a strain gauge under different loading levels, the strain value of the gauge can be obtained on the basis of its rating curve (Zhang et al. 2011). Because the steel bar can be considered completely bonded with the concrete, the strain in the concrete is assumed to be equal to that in the steel rebar. The axial force at shaft section *i* can be obtained according to Eq. (1). The distributions of axial forces of TS2 and TS3 before and

after grouting at different loading levels are shown in Figs. 9 and 10.

$$F_i = \frac{\varepsilon_{1i} + \varepsilon_{2i} + \varepsilon_{3i} + \varepsilon_{4i}}{4} (E_s A_s + E_c A_c) \tag{1}$$

where *F_i* is the axial force at shaft section *i* (kN), ε_{1i} , ε_{2i} , ε_{3i} and ε_{4i} are the strains of the symmetrical strain gauges at shaft section *i*, *E_s*, and *E_c* are the moduli of elasticity of the steel rebar and concrete (kPa), respectively, and *A_s* and *A_c* are the cross-sectional areas of the steel rebar and concrete (m²), respectively.

It can be observed from Figs. 9 and 10 that the axial force distribution of the shaft obtained by the bi-direction O-cell test method is different from that obtained by the top-down load test method. The distribution curve of the axial force of the shaft under the bi-direction O-cell test method is bounded by the position of the O-cell, and decreases gradually toward both ends of the shaft. The distribution curve of the axial force of the shaft under the top-down load test method is nearly trapezoidal along the shaft, and decreases from the shaft head to the shaft bottom. The axial forces of the test shafts before and after grouting decreases gradually toward both ends of the



◀ Fig. 9 Axial force distributions of test shaft TS2 before and after grouting at different loading levels

shaft because of the mobilization of shaft resistance and increase with increasing applied load at the same depth. It should be noted that the decreases in amplitude of the axial force along the test shafts are different in different rock formations. This is the main cause of the different rock properties of various rock formations. It can also be observed that the slope of the axial force distribution curve of the test shafts after grouting is less than that of the test shafts before grouting, indicating that there are some discrepancies in the mobilization of the shaft resistance between the test shafts before and after grouting. Consequently, the smaller is the slope, the greater is the shaft resistance.

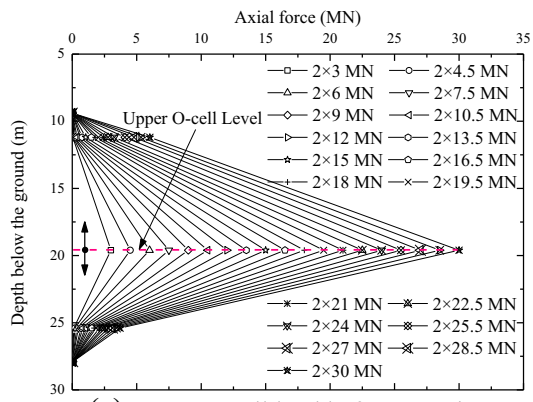
Mobilized shaft resistance

The shaft resistance is affected by the soil and rock properties, the relative displacement between pile and soil and the shaft-forming technology (Feng et al. 2016). Based on the axial force of the shaft and the parameters of the shaft section, the shaft resistance of the different soil layers is determined by Eq. (2). The distributions of shaft resistance for the test shafts TS2 and TS3 before and after grouting are shown in Figs. 11 and 12.

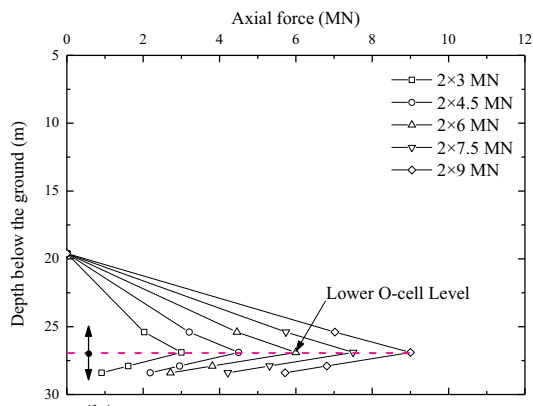
$$\tau_i = \frac{F_i - F_{i+1}}{\pi D L_i} \tag{2}$$

where τ_i is the side resistance at section i (kPa), D is the shaft diameter (m), and L_i is the length of the shaft in soil layer i (m).

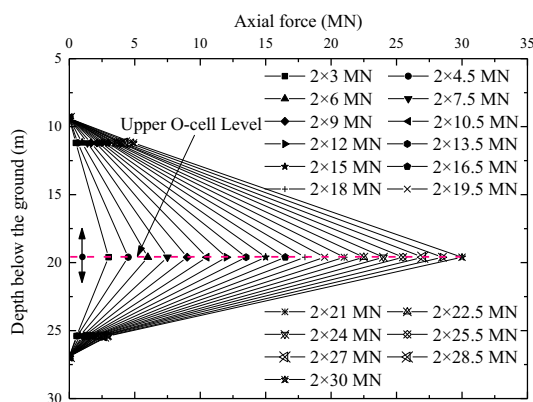
It can be found from Figs. 11 and 12 that the mobilized shaft resistance of the test shafts before and after grouting increases with increasing applied load, and the mobilized shaft resistance of the test shafts in the rock layers adjacent to the O-cell is greater than that of the test shafts in the rock layers away from the O-cell. That is, when the O-cell is loaded to the maximum load, the side resistance of the upper shaft segment has not been fully developed, indicating that the actual ultimate side resistance of the upper shaft segment is larger than the side resistance obtained by this test. The figures further show that the bearing capacity of the test shafts has a greater margin of capacity. In addition, the side resistance of the ungrouted shafts in the upper rock layers is similar to that of the grouted shafts, whereas that of the rock layers 5-1b, 5-1c, 7-1, and 7-2 surrounding grouted shafts is higher than that of the ungrouted shafts. For example, between the depths of 27.9 and 29.4 m, the maximum shaft resistance values observed were 465 and 565 kPa for the test shaft TS3 before and after grouting, respectively. Similarly, between the depths of 80 and 84 m, the maximum shaft resistance values observed were 747 and 807 kPa for the test shaft TS2 before and after grouting.



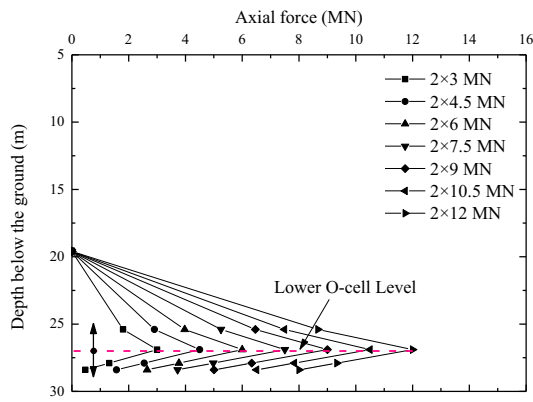
(a) Upper O-cell load before grouting



(b) Lower O-cell load before grouting



(c) Upper O-cell load after grouting



(d) Lower O-cell load after grouting

◀ Fig. 10 Axial force distributions of test shaft TS3 before and after grouting at different loading levels

As a conclusion, the shaft resistance of the test shafts after post-grouting was obviously improved.

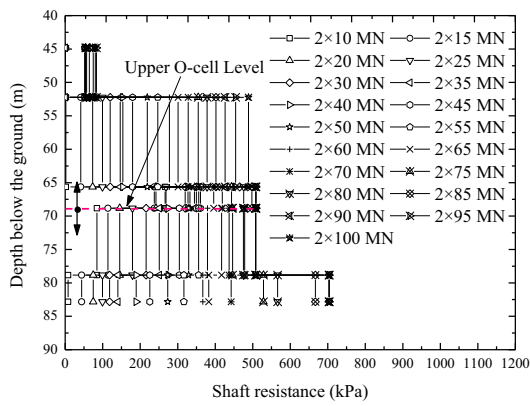
The relative displacement between the shaft and soil is an important factor affecting the shaft resistance that will eventually affect the ultimate bearing capacity and displacement of the shaft. Unfortunately, it is quite difficult to determine the displacement between the shaft and soil. Hence, it is assumed that the soil displacement is not affected by the shaft displacement. That is, the relative displacement between the shaft and soil at a specified depth is equal to the shaft displacement at the same depth. To study the effect of shaft-soil relative displacement on the shaft resistance, its value in different soil layers can be obtained with Eq. (3). The relationships between shaft resistance and shaft-rock relative displacement for test shafts TS2 and TS3 before and after grouting at different depths are shown in Figs. 13 and 14.

$$s_i = s_t - \sum_{j=1}^i \frac{L_j(F_j + F_{j+1})}{2E_P A_P} \quad (3)$$

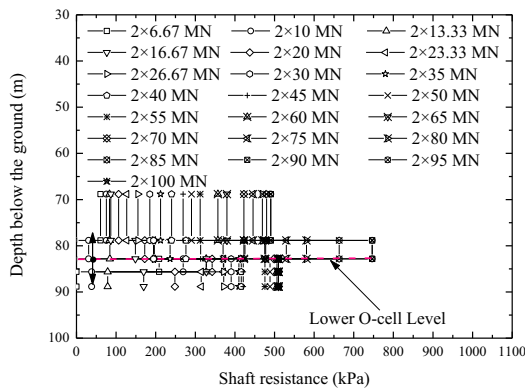
where s_i is the shaft-soil relative displacement between the soil layer i and shaft, s_t is the upward or downward displacement of the O-cell, E_P is the elastic modulus of the shaft (kPa), and A_P is the cross-sectional area of the shaft (m^2).

The Figs. 13 and 14 show that the shaft resistance of the test shafts increases rapidly at small relative displacement, and the shaft resistance increases nonlinearly as the relative displacement increases. The shaft resistance of the upper shaft segment for the test shafts is not fully mobilized, whereas the shaft resistance of the lower shaft segment develops rapidly and transitions into the plastic state. Moreover, the rock layers 4-2, 5-1b, and 7-2 show a strong potential shaft resistance due to the curve shape presented. The shaft-rock relative displacement required for the ultimate shaft resistance in different rock formations is not the same. Thus, when the shaft resistance of each rock formation reaches the maximum value, the required shaft-rock relative displacement is shown in Table 4.

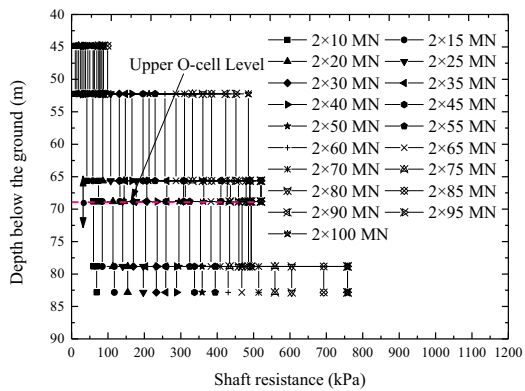
It can be observed from Table 4 that the shaft-rock relative displacement required for the development of the ultimate shaft resistance of grouted shafts is smaller than that of the ungrouted shafts, which indicates that post-grouting technique can effectively reduce the displacement of the shaft. It is noted that because of the small amount of cement pressed into the first ring-shaped grouting pipes at the side of the test shaft TS2, the influence of the upper rock layers on the shaft resistance is not obvious, which shows that the side grouting is not sufficient. Consequently, the amount of grout was the main factor affecting the grouting effect. Additionally, the shaft resistances of the middle and lower shaft segments for the test shafts TS2 and TS3 after grouting were obviously improved,



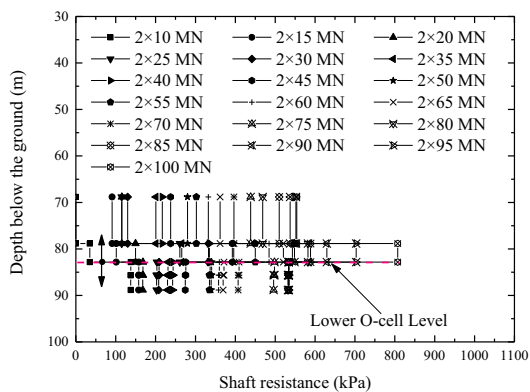
(a) Upper O-cell load before grouting



(b) Lower O-cell load before grouting



(c) Upper O-cell load after grouting



(d) Lower O-cell load after grouting

◀ Fig. 11 Distribution of shaft resistance for test shaft TS2 before and after grouting

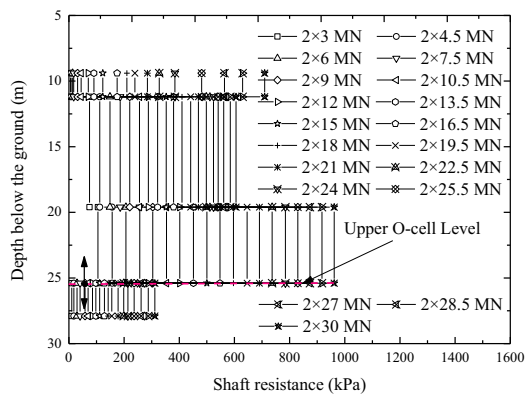
and the increased ranges of the shaft resistance in rock layers 5-1c, 7-1, and 7-2 were 21.51%, 12.83% and 8.03%, respectively. It is further suggested that the post-grouting technique can effectively enhance the shaft resistance in coral-reef limestone formations.

Mobilized tip resistance

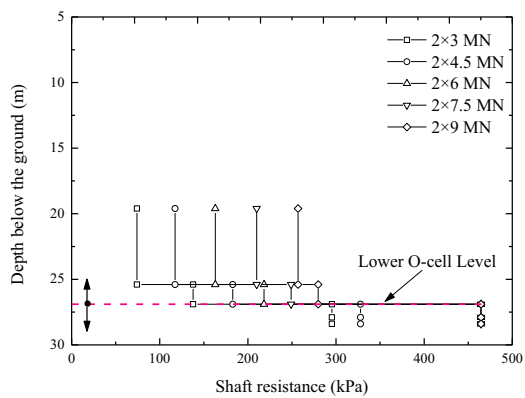
The tip resistance of a test shaft is obtained by subtracting the side resistance of the lower shaft segment from the lower O-cell load, whereas the tip displacement is obtained by subtracting the compression of the lower shaft segment from the downward displacement of the lower O-cell load. Thus, the tip resistance-displacement curves can be obtained, as shown in Fig. 15. Figure 15 shows that the trends of tip resistance-displacement curves for both shafts before grouting are similar to those for both shafts after grouting. The tip displacements for both shafts after grouting are smaller than those for both shafts before grouting at the same tip resistance, which indicates that end bearing capacity can be mobilized with smaller displacement after grouting. Reef rock formations at the shaft tip and the surrounding formations are crushed due to the drilling process, resulting in a loose and crushed structure. The pressurized grout compacts and penetrates the loose and crushed structure at the shaft tip and mixes with the crushed particles to effectively strengthen them, making them stronger and stiffer. Additionally, the shaft tip displacement decreases by 41 mm in this case due to the preloading effect of base grouting. This also reflects that the effect of tip grouting is significant, and that the bearing performance of the shaft tip is obviously improved.

Discussion

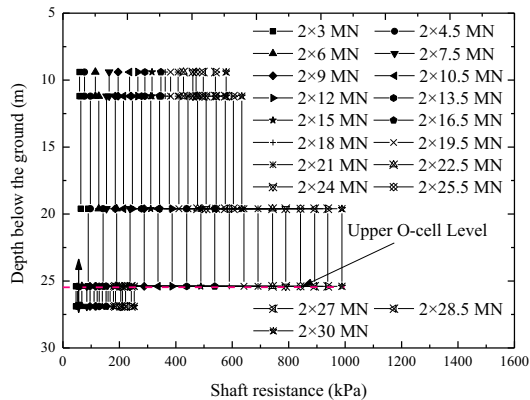
The test results have demonstrated that the two large-diameter drilled shafts in coral-reef limestone formations have high load-bearing capacity. For the test shaft TS2, the equivalent shaft head load-displacement curve reached the limit state because the upper, middle and lower shaft segments were loaded to the failure load; for the test shaft TS3, the expected ultimate load at the shaft head was not obtained due to the upper O-cell reaching its load limit, but the measured relationship between the tip resistance and tip displacement was obtained because the lower shaft segment was loaded to the failure load. Therefore, the ratios of the mobilized tip resistance or total shaft resistance to the shaft head load is discussed only for the test shaft TS2. The ratios of the mobilized tip resistance or total shaft resistance to the shaft head load for shaft TS2 before and after grouting under different



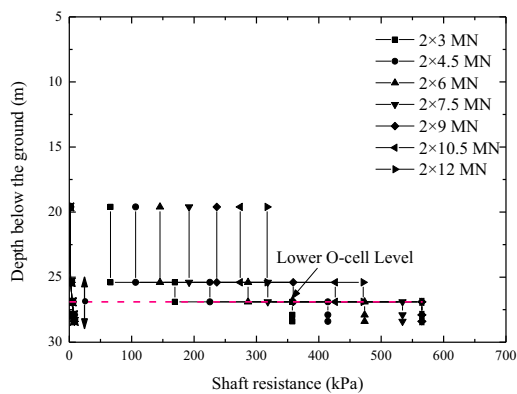
(a) Upper O-cell load before grouting



(b) Lower O-cell load before grouting



(c) Upper O-cell load after grouting

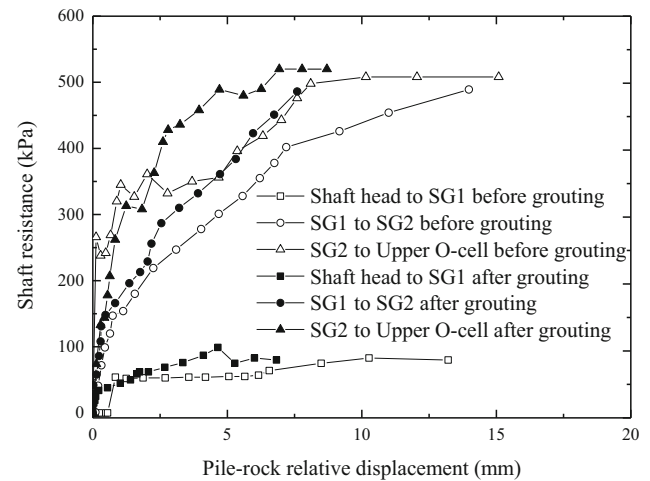


(d) Lower O-cell load after grouting

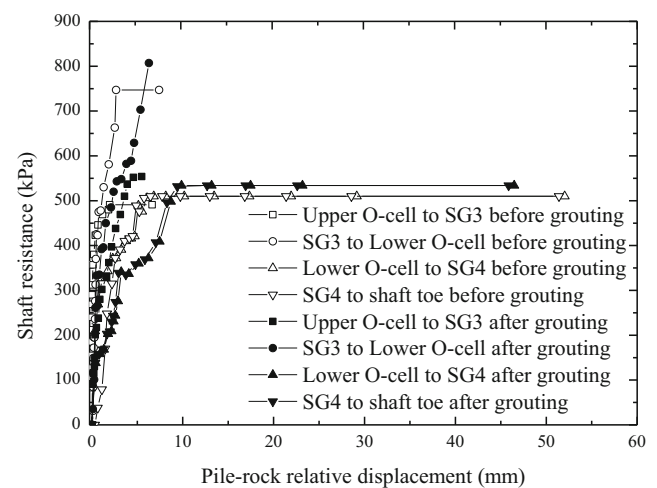
◀ Fig. 12 Distribution of shaft resistance for test shaft TS3 before and after grouting

loading levels are illustrated in Fig. 16. The ultimate load, total shaft resistance, and mobilized tip resistance for shaft TS2 are shown in Table 5.

It can be observed from Fig. 16 that the shaft head load for the test shaft TS2 before grouting is fully supported by the shaft resistance for small applied loads before the tip resistance was mobilized, whereas the shaft head load after grouting was first supported by the tip resistance during the initial load due to the preloading effect of tip grouting. With increasing applied load, the tip resistance was mobilized gradually, and the mobilized tip resistance sharing ratio Q_b/Q_u also gradually increased. As the applied load reached the ultimate load, the mobilized tip resistance sharing ratio was 21.52% and 20.21% for the test shaft TS2 before and after grouting,

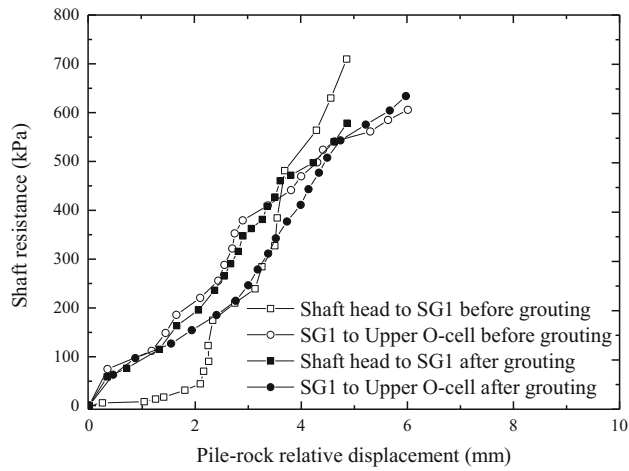


(a) Upper shaft segment

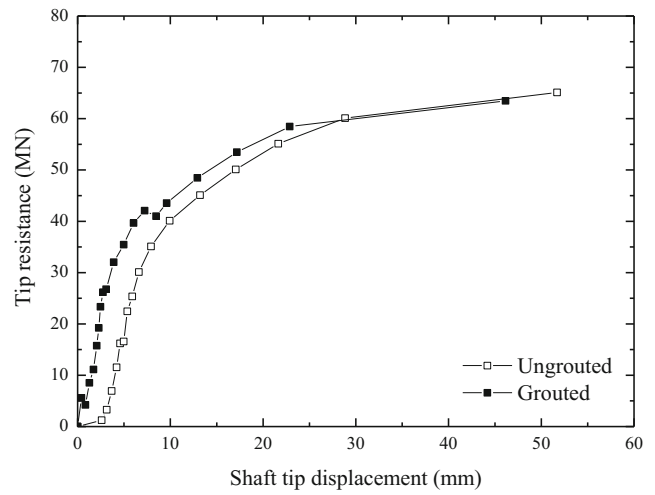


(b) Middle and lower shaft segment

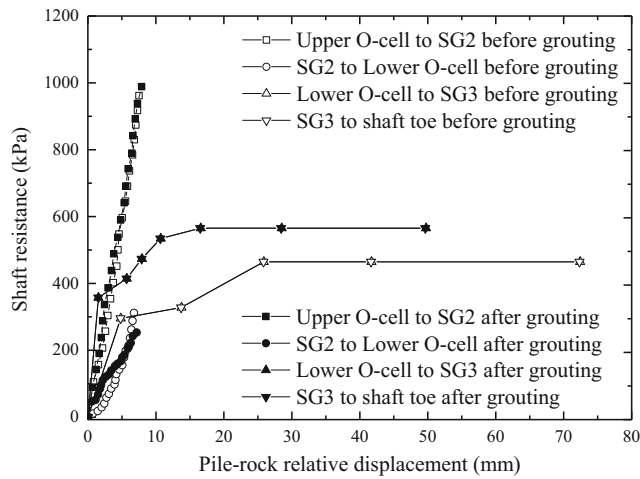
Fig. 13 Relationship between the shaft resistance and the relative displacement of test shaft TS2 before and after grouting



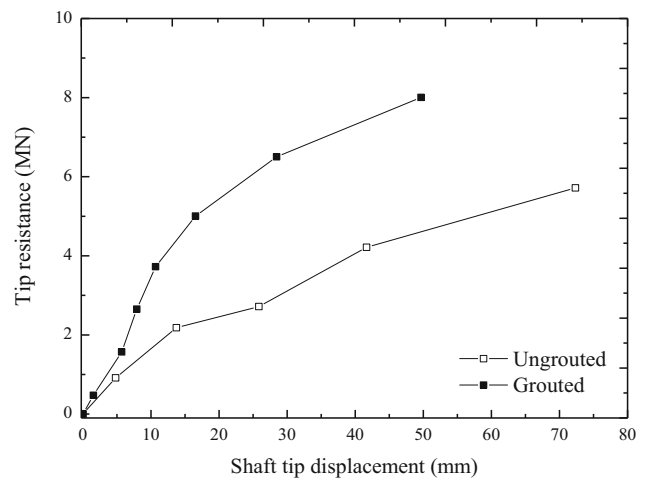
(a) Upper shaft segment



(a) TS2



(b) Middle and lower shaft segment



(b) TS3

Fig. 14 Relationship between the shaft resistance and the relative displacement of test shaft TS3 before and after grouting

Fig. 15 Relationship between the tip resistance and displacement of test shafts before and after grouting

Table 4 Shaft resistance and the relative displacement of test shafts

Shaft no.	Soil no.	Depth (m)	UngROUTED		Grouted		Improvement proportion of shaft resistance (%)
			Measured maximum shaft resistance (kPa)	Corresponding displacement (mm)	Measured maximum shaft resistance (kPa)	Corresponding displacement (mm)	
TS3	4-1	10.4-12.2	710	4.86	578	4.86	N/A
	4-2	12.2-20.6	606	6.01	634	5.97	4.62
	5-1b	20.6-26.4	962	7.51	989	7.89	2.81
	5-1c	26.4-27.9	312	6.76	253	7.16	N/A
	5-1c	27.9-29.4	465	41.68	565	28.47	21.51
TS2	6-2	46.0-54.0	80	13.21	80	6.83	N/A
	6-3	54.0-66.8	498	13.98	486	7.60	N/A
	6-3	66.8-70.0	508	15.09	520	8.70	2.36
	7-1	70.0-80.0	491	6.24	554	5.48	12.83
	7-2	80.0-84.0	747	7.01	807	6.28	8.03
7-1	84.0-90.0	510	28.84	534	22.89	4.71	

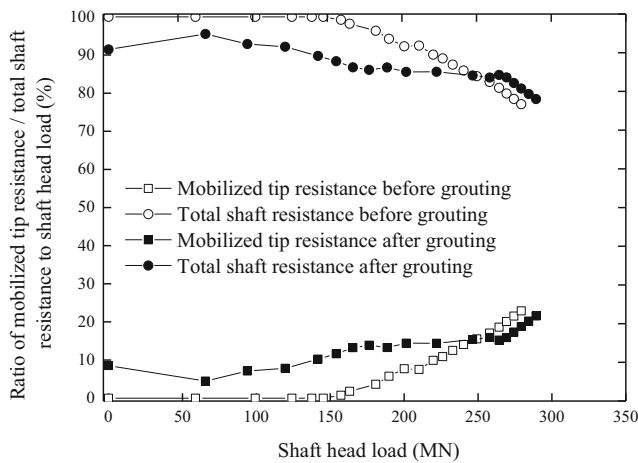


Fig. 16 Ratio of mobilized tip resistance/ total shaft resistance to shaft head load for test shaft TS2 before and after grouting at different loading levels

respectively. Hence, the large-diameter drilled shaft TS2 before and after grouting functioned as an end-bearing friction shaft. However, as shown in Fig. 16 and Table 5, the tip resistance for TS2 after grouting at the ultimate load was slightly less than that for TS2 before grouting. This result may be caused by the fact that the strength of the cement grout did not meet the requirements, or that the tip grouting to enhance the tip resistance was not obvious because of the larger tip resistance capacity. It is noted that under the service load (which is generally half of the ultimate load), the tip displacement for TS2 after grouting was less than that before grouting at the same tip resistance. Additionally, the total shaft resistance at the ultimate load for TS2 after grouting was larger than that before grouting. The mobilized unit shaft resistance for TS2 after grouting was also larger than that before grouting, as shown in Table 4. The findings indicate that the post-grouting technique of the shaft tip-and-side combination can effectively enhance the mobilization of shaft resistance in coral-reef limestone formations.

Figure 17 shows the relationships between the mobilized unit tip resistance and normalized tip displacement for the test shafts before and after grouting. The normalized tip displacement is the ratio of the tip displacement to the shaft diameter (D). As previously described, the tip displacement s_t is obtained by subtracting the compression of the lower shaft segment from the downward displacement of the lower O-cell load and is normalized by D . In Fig. 17, the mobilized unit tip

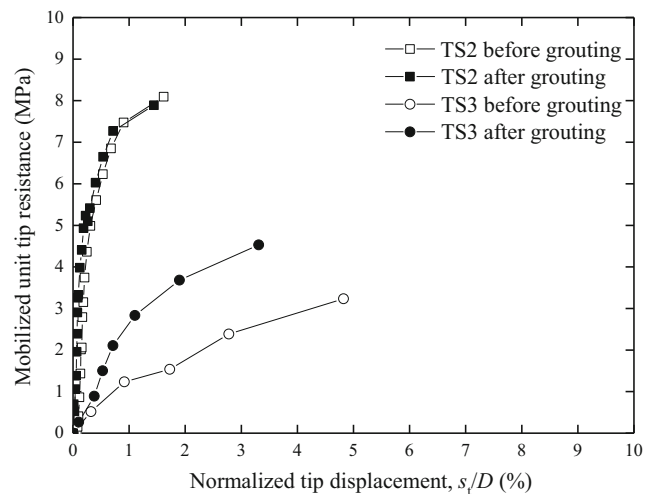


Fig. 17 Relationships between the mobilized unit tip resistance and normalized tip displacement of test shafts before and after grouting

resistance increases with increasing normalized tip displacement. The mobilized unit tip resistance for the test shafts after grouting is larger than that for the test shafts before grouting at the same normalized tip settlement, especially for the test shaft TS3. It should be noted that the tip displacement for the fully mobilizing tip resistance capacity of test shaft TS3 in the reef rock with cavity layers before and after grouting was 3%–5% of D , whereas the tip displacement for the fully mobilizing tip resistance capacity of test shaft TS2 in the crushed reef rock with gravel layers before and after grouting was 1%–2% of D . This normalized tip displacement for the fully mobilizing tip resistance (i.e., 3%–5%) is consistent with the value of 4%–5% reported by Reese and O’Neil (1988), but smaller than the 6–12% described by Liu et al. (2017). The tip displacement needed to mobilize ultimate tip resistance ranges may result from the different bearing stratum, the size shaft, the construction uncertainty of each shaft, and the effect of post-grouting (Ng et al. 2001; Liu et al. 2017).

In addition, much of the literature (Angemeer et al. 1973; Hagenaar 1982; Dutt and Cheng 1984; Gilchrist 1985) has reported that the measured shaft resistance in calcareous sediments was very low through the driven shaft test and because the cementation structures were destroyed, and a large number of particles were broken during the piling process, reducing effective stress in the vertical and horizontal directions. However, shaft resistance is an important component of the bearing capacity of shaft foundations. The ultimate bearing

Table 5 Bearing capacity analysis at the ultimate test shaft load before and after grouting

Shaft no.	Grouting situation	Q_u (MN)	Q_{su} (MN)	Q_{bu} (MN)	Q_{bu} / Q_u (%)	q_{bu} (MPa)
TS2	UngROUTED	279.29	219.19	60.10	21.52	7.47
	Grouted	289.29	230.82	58.47	20.21	7.27

Note: Q_u is the ultimate bearing capacity of the test shafts; Q_{bu} is the mobilized tip resistance of the test shafts; Q_{su} represents the total shaft resistance of the test shafts, which is obtained by subtracting the mobilized tip resistance from the ultimate bearing capacity; and q_{bu} is the unit tip resistance of the test shafts

capacity of a traditional driven shaft is thus very low and cannot meet the engineering requirements. Based on the abovementioned issues, some scholars have proposed a drilled and grouted shaft, and conducted model shaft tests or field tests to explore its bearing characteristics; the findings show that the measured average shaft resistance in unconsolidated calcareous soil is approximately 100 kPa (Wees and Chamberlin 1971; Beringen et al. 1982; Nauroy et al. 1985). In this study, the measured shaft resistance was much larger than the measured shaft resistance in the literature. This shows that the coral-reef limestone formations in this area have high shaft resistance. It also further reflects that coral-reef limestone has regional characteristics. Furthermore, the post-grouting technique can be applied to coral-reef limestone formations and can improve its bearing capacity through enhancing both the tip and shaft resistances. Therefore, increasing tip and shaft resistance of large diameter shafts in coral-reef limestone formations with post-grouting is an effective method to improve shaft bearing capacity. It is recommended that post-grouting techniques be used in the installation of shaft foundations in coral-reef limestone formations, especially for large diameter and super-deep drilled shafts.

Conclusions

This paper reports two full-scale load tests conducted on the coral-reef limestone formations of the Male-Airport Island Cross-sea Bridge area in the Maldives to investigate the field performance of large-diameter drilled shafts before and after grouting. From the test analyses and discussions of the grouted and ungrouted shafts, the following conclusions can be drawn.

- (1) The bearing capacities of large-tonnage drilled shafts before and after grouting in the Male-Airport Island Cross-sea Bridge were successfully tested with the bi-directional O-cell test method. The results show that the reef limestone formations in this area have high bearing capacity; the bearing capacities of both shafts fully meet the requirements of the design load, and also have a greater surplus capacity.
- (2) Post-grouting can be applied to coral-reef limestone formations and can effectively improve the bearing capacity of a shaft foundation and decrease its settlement. According to equivalent conversion results before and after grouting, the shaft head displacements were reduced by 33.53% and 17.34% due to the combined grouting and the tip grouting, respectively, indicating that the combined grouting at the shaft tip and side to reduce the shaft head settlement is more effective than grouting at the shaft tip alone.

- (3) The ultimate shaft resistance for test shafts after grouting is larger than that for test shafts before grouting under the same conditions. The post-grouting technique can effectively increase the shaft resistance through enhancing adhesion of the concrete to the coral-reef limestone formation.
- (4) The shaft resistance in the upper rock layers was not fully mobilized, whereas the shaft resistance in the lower rock layers developed rapidly and went into the plastic state. Consequently, this phenomenon shows that the shaft-rock relative displacement needed to achieve the ultimate shaft resistance is not the same in different rock layers.
- (5) The tip resistances of the test shafts after grouting were significantly mobilized and larger than those of the test shafts before grouting. Under the ultimate load, the mobilized tip resistances of test shaft TS2 before and after grouting were 7.47 and 7.27 MPa (at the tip displacement of 1%–2% D), respectively, whereas the mobilized tip resistances of test shaft TS3 before and after grouting were 2.39 and 3.68 MPa (at the tip displacement of 3%–5% D), respectively. Compared with the test shafts before grouting under the service load, the tip displacements for the test shafts after grouting were obviously reduced.
- (6) The research results are to be applied in the shaft design of the Male-Airport Island Cross-sea Bridge to solve its difficulties and to achieve a remarkable economic benefit. The results also may be applicable to similar projects in coral-reef limestone formations.

Acknowledgements The authors are very grateful to the reviewers for their helpful comments and constructive suggestions in improving this paper.

Funding This work was supported by the major state Basic Research Development Program of China (973 program) (No. 2013CB036304), and the National Natural Science Foundation of China (No. 51678145).

References

- Wees JA, Chamberlin RS (1971) Khazzan Dubai no. 1: Pile design and installation. *J Soil Mech Found Div* 97(10):1415–1429
- Angemeer J, Carlson E G, Klick J H. Techniques and results of offshore pile load testing in calcareous soils. *Offshore Technology Conference*. Offshore Technology Conference, 1973
- Bolognesi AJL, Moretto O (1973) Stage grouting preloading of large piles on sand. *Proceedings of 8th ICSME*. Moscow 2(1):19–25
- O'Neill M W and Reese L C. Behavior of axially loaded drilled shafts in clay-shales. *Center for Highway Research*. The University of Texas at Austin. 1976
- Agarwal SL, Malhotra AK, Banerjee RL (1977) Engineering properties of calcareous soils affecting the design of deep penetration piles for offshore structures. *Proc, 9th Int Offshore Technol Conf*. Houston, USA 3:503–512
- Sliwinski Z J and Philpot T A. Conditions for effective end-bearing of bored cast in-situ piles. *Proceedings ICE Conference on recent developments in the design and construction of pile*, 1980: 73–80

- Beringen FL, Kolk HJ, Windle D (1982) Cone penetration and laboratory testing in marine calcareous sediments. *ASTM STP 777*:179–209
- Hagenaar J. The use and interpretation of SPT results for the determination of axial bearing capacities of piles driven into carbonate soils and coral. *Proc 2nd Europe0 Symp Penetration Test, Amsterdam, the Netherlands. 1982*: 51–55
- Dutt R N, Cheng A P. Frictional response of piles in calcareous deposits. *Offshore Technology Conference Offshore Technology Conference, 1984*
- Sliwinski Z J, Fleming W G K. The integrity and performance of bored piles. *Piling and ground treatment. Thomas Telford Publishing, 1984*: 211–223
- Deshmukh AM, Gulhati SK, Roa GV et al (1985) Influence of geological aspects on behaviour of coral rock. *11th Int Conf Soil Mech Found Eng, San Francisco, USA 5*:2397–2400
- Gilchrist JM (1985) Load tests on tubular piles in coralline strata. *J Geotech Eng 111(5)*:641–655
- Nauroy J F, LeTirant P. Driven piles and drilled and grouted piles in calcareous sands. *Offshore Technology Conference Offshore Technology Conference, 1985*: 83–91
- Bruce DA (1986) Enhancing the performance of large diameter piles by grouting. *Ground Eng 19(4)*:9–15
- Osterberg J O. Device for testing the load-bearing capacity of concrete-filled earthen shafts: U.S. Patent 4,614,110. 1986–9–30
- Ghazali F M, Baghdadi Z A, and Mansur O A. A Comparative Study of Pile Foundations in Coral Formations and Calcareous Sediments in the Red Sea. *9th South East Asian Conference, Bangkok, Thailand, 1987*
- Ghazali FM, Sotiropoulos E, Mansour OA (1988) Large-diameter bored and grouted piles in marine sediments of the Red Sea. *Can Geotech J 25(4)*:826–831
- Reese L C, O'Neill M W. *Drilled shafts: Construction and design*. FHWA, Publication No. HI-88, 1988, 42
- Poulos H G. *The mechanics of calcareous sediments*. University of Sydney, School of Civil and Mining Engineering, 1989
- Hirayama H (1990) Load-settlement analysis for bored piles using hyperbolic transfer functions. *Soils Found 30(1)*:55–64
- Prakash S, Sharma HD (1990) *Pile foundations in engineering practice*. John Wiley & Sons, New York, USA
- Majano RE, O'Neill MW, Hassan KM (1994) Perimeter load transfer in model drilled shafts formed under slurry. *J Geotech Eng 120(12)*: 2136–2154
- Gunasena U, Jeer H A, Randolph M F. Design approach for grouted driven piles in calcareous soil. *Offshore Technol Conference, 1995*: 271–280
- Wang R, Song CJ, Zhao HT et al (1997) *Coral reef engineering geology of Nansha Islands*. Science Press, Beijing (in Chinese)
- Joer H A, Randolph M F, Gunasena U. Experimental modeling of the shaft capacity of grouted driven piles. *Geotech Test J, 1998*: 159–168
- Mullins G, Dapp S D, Lai P. Pressure-grouting drilled shaft tips in sand. *New technological and design developments in deep foundations, 2000*: 1–17
- Ng CWW, Yau TLY, Li JHM et al (2001) New failure load criterion for large diameter bored piles in weathered geomaterials. *J Geotech Geoenviron 127(6)*:488–498
- Mullins G, Dapp S, Frederick E et al (2001) *Post grouting drilled shaft tips: phase I. Research Report University of South Florida, Tampa, USA, pp 127–156*
- Dapp S D, Mullins G. Pressure grouting drilled shaft tips: Full-scale research investigation for silty and shelly sands. *Deep Foundations: An International Perspective on Theory, Design, Construction, and Performance. 2002*: 335–350
- Dapp S D, Muchard M, and Brown D A. Experiences with base grouted drilled shafts in the Southeastern United States. *Proceedings of 10th international conference on piling and deep foundations, 2006*: 1385–1394
- Mullins G, Winters D, Steven D (2006) Predicting end bearing capacity of post-grouted drilled shaft in Cohesionless soils. *J Geotech Geoenviron 132(4)*:478–487
- Safaqah O, Bittner R, Zhang X G. Post-grouting of drilled shaft tips on the Sutong Bridge: a case study. *Proceedings of Geo-Denver 2007 Congress: Contemporary Issues in Deep Foundation, 2007*
- Duan X and Kulhawy F H. Tip post-grouting of slurry-drilled shafts in soil: Chinese experiences. *Contemporary topics in deep foundations, 2009*: 47–54
- The Traffic Professional Standards Compilation Group of People's Republic of China (2009) *JT/T 738–2009 static loading test of foundation pile-self-balanced method*. China Communications Press, Beijing (in Chinese)
- Zhang ZM, Yu J, Zhang GX et al (2009) Test study on the characteristics of mudcakes and in situ soils around bored piles. *Can Geotech J 46(3)*:241–255
- Dai G, Gong W, Zhao X et al (2010) Static testing of pile-base post-grouting piles of the Suramadu bridge. *Geotech Test J 34(1)*:34–49
- Zhang Z, Zhang Q, Yu F (2011) A destructive field study on the behavior of piles under tension and compression. *J Zhejiang Univ-Sci A 12(4)*:291–300
- Zhang Q, Zhang Z (2012) Complete load transfer behavior of base-grouted bored piles. *J Cent South Univ 19(7)*:2037–2046
- Thiyyakkandi S, McVay M, Bloomquist D et al (2014) Experimental study, numerical modeling of and axial prediction approach to base grouted drilled shafts in cohesionless soils. *Acta Geotech 9(3)*:439–454
- Zhang Q, Li SC, Li LP (2014) Field study on the behavior of destructive and non-destructive piles under compression. *Mar Georesour Geotechnol 32(1)*:18–37
- Liu NW, Gong XN, Yu F (2015) Vertical bearing capacity of large-diameter bored pile. *J Zhejiang Univ (Engineering Science) 49(4)*: 763–768
- Nguyen MH, Fellenius BH (2015) Bidirectional cell tests on non-grouted and grouted large-diameter bored piles. *Journal of Geo-Engineering Sciences 2(3, 4)*:105–117
- Choi Y, Lee MH, Nam MS et al (2016) Development and implementation of a high-pressure, double-acting, bi-directional loading cell for drilled shafts. *Geotech Test J 39(2)*:196–205
- Feng SJ, Lu SF, Shi ZM (2016) Field investigations of two super-long steel pipe piles in offshore areas. *Mar Georesour Geotechnol 34(6)*: 559–570
- Liu KF, Xie XY, Luo Z et al (2017) Full-scale field load testing of long drilled shafts with enlarged base constructed in marine sediment. *Mar Georesour Geotechnol 35(3)*:346–356